

Article

Not peer-reviewed version

---

# An Affordable Acoustic Measurement Campaign for Early Prototyping Applied to Electric Ducted Fan Units

---

[Stefan Schoder](#)\*, Jakob Schmidt, Andreas Furlinger, [Klaus Roppert](#), [Paul Maurerlehner](#)

Posted Date: 8 March 2023

doi: 10.20944/preprints202303.0142.v1

Keywords: Aeroacoustics; Electric ducted fan; Microperforated plate absorbers; eVTOL




Preprints.org is a free multidiscipline platform providing preprint service that is dedicated to making early versions of research outputs permanently available and citable. Preprints posted at Preprints.org appear in Web of Science, Crossref, Google Scholar, Scilit, Europe PMC.

Copyright: This is an open access article distributed under the Creative Commons Attribution License which permits unrestricted use, distribution, and reproduction in any medium, provided the original work is properly cited.

## Article

# An Affordable Acoustic Measurement Campaign for Early Prototyping Applied to Electric Ducted Fan Units

Stefan Schoder <sup>1,\*†‡</sup> , Jakob Schmidt <sup>2‡</sup>, Andreas Förlinger <sup>3</sup>, Roppert Klaus <sup>1</sup> and Maurerlehner Paul <sup>1</sup>

<sup>1</sup> TU Graz, IGTE, Graz, Austria, 8010; stefan.schoder@tugraz.at

<sup>2</sup> TU Wien, Wien, Austria, 1040

<sup>3</sup> VOLARE GmbH, Mödling, Austria, 2340

\* Correspondence: stefan.schoder@tugraz.at (S.S.)

† Current address: Affiliation 1.

‡ These authors contributed equally to this work.

**Abstract:** New innovative green concepts in electrified vertical take-off and landing vehicles currently emerge as a revolution to urban mobility going into the third dimension (vertically). The high population density of cities makes the market share highly attractive while posing an extraordinary challenge for community acceptance due to the increasing and possibly noisier commuter traffic. In addition to passenger transport, package deliveries to customers by drones may enter the market. The new challenges associated with this increasing transportation need in urban, rural and populated areas pose challenges for established companies and startups to deliver low-noise emission products. The article's objective is to revisit the benefits and drawbacks of an affordable acoustic measurement campaign focused on early prototyping. In the very early phase of product development, often considerably limited resources are available. With this in mind, the article discusses the sound power results using the enveloping surface method in a typically available low-reflection room with a reflecting floor according to *DIN EN ISO 3744:2011-02*. The method is applied to a subsonic electric ducted fan (EDF) unit of a 1:2 scaled electrified vertical take-off and landing vehicle. The results show that considerable information at low costs can be gained for the early prototyping stage, despite this easy-to-use, easy-to-realize, and not fine-tuned measurement setup. Furthermore, the limitations and improvements to a possible experimental setup are presented to discuss a potentially more ideal measurement environment. Measurements at discrete operating points and transient measurements across the total operating range were conducted to provide complete information on the EDF's acoustic behavior. The rotor-self noise and the rotor-stator interaction were identified as primary tonal sound sources, along with the highest broadband noise sources located on the rotor. Based on engineering experience, a first acoustic improvement treatment is also quantified with a sound power level reduction of 4dB(A). In conclusion, the presented method is a beneficial first measurement campaign to quantify the acoustic properties of an electric ducted fan unit at minimal resources in a reasonable time of several weeks when starting from scratch.

**Keywords:** Aeroacoustics; electric ducted fan; microperforated plate absorbers; eVTOL

## 1. Introduction

Highly populated cities make the market share of transportation and product deliveries for urban mobility extremely attractive by going into the third dimension (vertically). The demand for fast relocation is met by (electrified) vertical take-off and landing vehicles for passenger transport, and drones possibly deliver goods in the future. It is evident that this scenario poses an extraordinary challenge for the community issuing regulations (ICAO Annex 16 [1]) and the stakeholders of such operating systems due to possible noise emissions that must be classified, analyzed and reduced to an acceptable minimum [2]. The article revisits the usefulness of a measurement procedure to gain first

insights into such propulsion units associated with new disruptive technologies and outlines how to start with noise mitigation at the early prototyping stage affordably and within a short time.

Electric propulsion has become a vital part of the aviation sector among electrically powered vertical take-off and landing (eVTOL) aircraft. Noise emissions of those eVTOL aircraft are mainly produced by the propulsion and lifting units and are of major concern during certification. During vertical flight operation, usually performed in urban and rural areas, the propulsion units' thrust generates lift forces [3,4] and, simultaneously, a substantial amount of noise emissions. One type of an electric propulsion system is an EDF. Figure 1 shows a schematic of the EDF based on a single-stage axial fan and its aerodynamic and electric components. Such an EDF is the subject of this study on acoustic characterization in early prototyping.

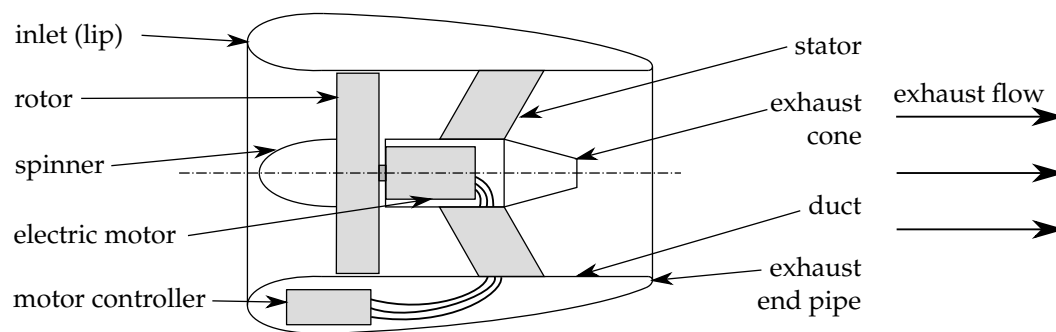


**Figure 1.** Visualization of components in a typical single-stage axial-flow EDF unit. Adapted from [5].

Similar types of electric aero-engines [6–10] have been studied for small-scale aircrafts aerodynamically [11]. Typically, the rotors are driven at high angular velocities (like 8000 revolutions per minute) and relatively low Reynolds numbers (10.000 to 100.000) compared to large aircraft engines. Both the positioning of multiple propulsion units as well as the in-duct placement of the rotors is a challenge for flight control and noise [4,11] but offers a high potential for optimization of fuel consumption, emission, noise reduction [12–14], and operational flexibility [15]. Although the whole aircraft offers acoustic shielding effects, in early prototyping, a component-based evaluation is of significant importance to detect design errors upfront [16] and gain experience with electric propulsion units [17].

Concerning this need for structured experimental assessment of preliminary design at low cost, this case study on the electric ducted fan unit provides valuable insights for conducting such evaluation with relatively few resources and within a stringent timeframe. In contrast to well-tailored and detailed experimental studies concerning electric ducted fan noise [18,19] of the past hosted inside expensive facilities, the study concentrates on the overall aspects and an easy-to-realize and affordable method also during the starting phase of a new idea with a limited budget. In [18], the aeroacoustic aspects of the design, construction, and testing of an all-electric ducted fan propulsion unit inside a large anechoic test chamber are presented. In general, ducted fan configurations potentially reduce noise emissions significantly [19–21]. These options include incorporating acoustic liners to the ducted walls [22] and designing the ratio of stator vanes to rotor blades so that specific blade passing frequency harmonics are cut-off [23]. Recently, studies showed insignificant or even noise amplification can occur when incorporating simple ducts into an existing propeller unit [11,12]. The duct as a design concept having both a potential to lower or increase the sound emission is critical; possible erroneous designs can be sorted out early with the proposed method since keeping them in the development process is very costly. Furthermore, the method can be combined with computational models [24,25] to gain further insight into the mechanism and serve as a plausible baseline for the simulation.

Another important aspect of the noise generation of electric ducted fans is the excitation of electric motor forces and a possible attenuation by structural modes [26]. Additionally, the authors of [22] reported high-frequency noise of the electronic switching since the frequencies can be close to natural

frequencies of the structure, especially when placed inside the fan's duct. Typically, this switching noise occurs around a base switching frequency, and both increasing and falling harmonics arise during operation [26–28]. Common strategies for avoiding this source of sound are placing them outside the human hearing range or by advanced switching algorithms [27]. For instance, such a parasitic side effect is an exemplary motivation for this article by the underlying data showing unexpected effects of the electric drive of the electric ducted fan unit.

Based on the proposed enveloping surface of the international standard *DIN EN ISO 3744:2011-02*, ten microphones were positioned around the electric ducted fan unit. The fan's sound emissions are subject to the following investigation at different operating points. The total sound power of the operating EDF unit was measured at different operation points. In doing so, far-field measurements of the unit's electric powertrain with and without load were conducted, which showed significant noise emissions at the blade passing frequencies. We investigate acoustically the electric powertrain, consisting of an electronically commutated brushless DC motor (ECM) and the motor controller without load and found significant contributions from the periodic electromagnetic forces and the motor controller electronics. After processing the insights gained from the measuring campaign, a secondary noise reduction measure was designed. By considering several options for noise mitigation, a micro-perforated plate liner configuration after the fan was placed inside the duct with an optimally designed back volume. The noise was evaluated using an A-weighting to account for human perception. This paper is an extended version of an article published in the AIAA Aviation Forum 2021, Virtuall, USA, 2 Aug 2021-6 Aug 2021 [22].

The article is structured as follows. The electric ducted fan unit and the upfront noise mitigation measures are presented. Followed by the setup of the measurement campaign designed for early prototyping studies of electric ducted fan units. The limitation of the enveloping surface method regarding this application is discussed. Based on this initial measurement campaign, the results are analyzed, and conclusions for improvements are drawn in a structured way. The results indicate two interesting issues for further analysis. Firstly, at 9000 revolutions per minute, a hump in the overall sound pressure level was found and further investigated within the means of the method. Secondly, the characteristics of the far-field noise of the EDF unit's electric powertrain, consisting of a brushless DC motor and electronic speed controller, without load were analyzed. After processing the insights gained from the measuring campaign with accompanying duct mode simulations, a secondary noise reduction measure was designed and evaluated.

## 2. Application and device under test

The device under test is a subsonic, subscale 1:2, single-stage, axial-flow EDF unit. Figure 2 shows how the axial-flow EDFs are mounted at the APELEON X1 and provides a detailed picture of the EDF unit mounted on the propulsion test rig during the measurement setup of the enveloping surface method.



**Figure 2.** The device under test during the measurement campaign (right) is one fan of the propulsion assemblies, which are arranged left and right of the fuselage of the APELEON X1 (left).

Figure 1 schematically shows the structure of the EDF unit under test. The primary parts of the EDF unit are the rotor, consisting of 7 blades, the spinner, the electric motor, the stator with four guide vanes vectorizing the flow and connecting the brushless DC motor (7 pole pairs) with the motor controller, which is assembled inside the duct hub and the duct with a curved inlet lip. Further geometrical details can be found in [5].

2.1. Revisiting basic acoustic emissions of EDF units

This EDF unit generates aeroacoustic sound that is characteristic for axial fans [29] and summarized in Table 1.

**Table 1.** Aeroacoustic sources and characteristics in axial fans associated with the rotor, adapted from [5,29].

	mechanism	tonal	narrowband	broadband
rotor self-noise	blade thickness noise	■		
	Gutin noise	■		
	boundary layer noise			■
	boundary layer separation noise			■
	trailing edge (TE) noise (laminar BL)	■		
	TE noise (turbulent BL)	■		■
	blunt TE vortex shedding	■		
	tip noise			■
	turbulence ingestion (leading edge) noise			■
	unsteady loading noise	■		
	subharmonic tip noise		■	
	rotating stall		■	
	multiple pure tones	■		

According to [23], the primary noise emissions of axial fans stem from aerodynamic excitation. Rotor self-noise and noise generated by the interaction between the rotor and stator flow generate tonal noise at the blade passing frequency (BPF) [30,31]  $f_{BPF} = Bf_{rot}$ , and its harmonic frequencies  $f_{BPFn} = nf_{BPF}$ , with  $B$  being the number of rotor blades,  $f_{rot}$  the rotational speed, and  $n$  the harmonic multiplicity. The noise origin at the BPF and its harmonics is anticipated to be from the rotor-stator interactions for subsonic rotor-self mechanisms inside circular ducts [30].

In addition, the EDFs electric powertrain emits noise. Table 2 summarizes possible source and attenuation mechanisms related to the electric motor placement inside the duct. The individual mechanisms are classified into tonal and broadband representation inside a measured spectrum. Furthermore, the excitation is classified as aeroacoustic, structurally related, and electrodynamic. In addition, the electric drive parts, electronic commutate motor (ECM), and electronic speed controller (ESC), responsible for the acoustic emission, are also provided.

The noise emissions of an ECM are a result from electromagnetic force and torque ripples during operation [32–35]. The fundamental frequency of the electromagnetic force forces is  $f_{LF} = 2pf_{rot}$ , and its harmonic frequencies are  $f_{LFn} = 2npf_{rot}$ . The frequencies can be computed using the number of motor pole pairs  $p$  [32,34,35].



**Table 2.** Acoustic sources and characteristics in axial fans associated with the electric powertrain [5].

	mechanism	ECM	ESC	tonal	broadband
aeroac.	boundary layer noise	■	■		■
	vortex shedding	■	■	■	
	cavity resonance	■	■	■	
struct.	bearing noise	■		■	■
	ECM rotor unbalance	■		■	
	structural modes	■		■	
electrodyn.	tangential Lorentz force	■		■	
	normal Lorentz force	■		■	
	cogging torque	■		■	
	torque ripple	■		■	
	switching frequency		■	■	

2.2. Noise mitigation strategies

Since future small aircraft should operate and be tolerated in urban and rural environments, noise reduction is relevant, even on the component level. Therefore, propulsion noise should be considered early, indicating a motivation for this investigation at the conceptual design stage [15]. For instance, the ducted fan offers the potential of combining a variety of rotor blade and stator vane designs to minimize noise, offers noise shielding options, and the placement of acoustic liners [36,37]. Figure 3 shows possible locations to apply noise mitigation measures.

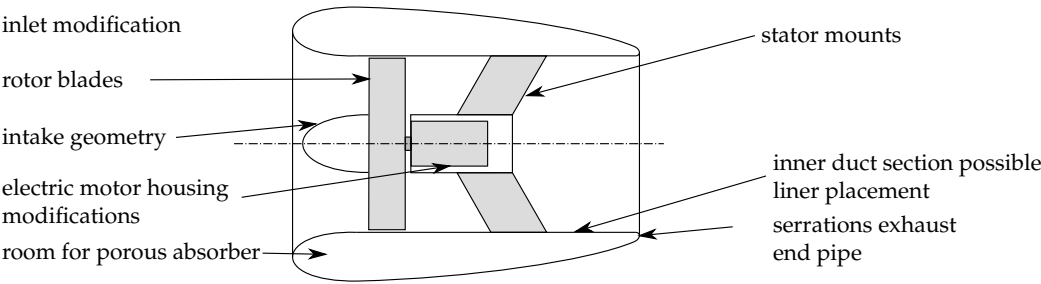


**Figure 3.** Visualization of potential noise reduction measures at an EDF unit.

In the current design, the stator is placed downstream, as so-called outlet guide vanes, to significantly lower sound pressure levels (SPL) for the resulting rotor-stator interaction compared to upstream stator installations [38]. The guide vanes are swept to decrease the noise emissions further. No special care was taken in the current configuration by selecting the rotor blade number and the guide vane number to cut off lower harmonic duct modes. Also, no modifications of the leading and trailing edge serrations [39] or forward and backward skew [40] were applied to the fan blades.

A possible noise amplification effect that is important to be investigated is that the manufactured EDF unit number of electric motor pole pairs equals the rotor blades  $p = B = 7$ . As a consequence, the excitation frequency of the electromagnetic forces matches the second harmonic of the BPF  $f_{LF} = 2f_{BPF}$  of the EDF unit. Changing this attribute can reduce the emitted sound regarding the overall sound level.

Finally, the electric motor controller cooling fins reach into the air stream inside the duct to achieve the required cooling. This placement impacts the overall aerodynamic sound generation. Furthermore, the structural sound of the switching currents may be transmitted inside the duct and possibly amplified. In the case of occurring switching noise, advanced switching routines can reduce the noise emissions drastically.

### 2.3. Design constraints for noise mitigation measures

Regarding this study, being executed in early prototyping, the primary and fundamental principles behind the noise generation are essential to gain a first insight into the aeroacoustic properties of the device [15]. In reality, the design space of possible noise mitigation structures was limited by the current design of the EDF unit. No alternation of the housing and dimensions of the duct with a length of 250 mm, a duct diameter of 201.3 mm, the number of stator blades and the number of rotor blades, and the rotor diameter of 200 mm was in the scope of possibilities. Furthermore, the influence of a possible treatment on the aerodynamic characteristics of the fan and the EDF unit must be kept to a minimum. Additionally, the position of the motor controller electronics must stay at the same place due to the cooling requirements. These constraints fundamentally reduced the design space for noise mitigation strategies. After an initial measurement campaign, an acoustic liner treatment to partly cover the inner duct side was applied for the first reduction measure for the acoustic emissions (see Figure 4). We selected to use micro-perforated (MASH of the company *fteu*) liners with back volume, among other treatments, since minor changes in the aerodynamic properties are expected and currently unused volume in the duct can provide value.

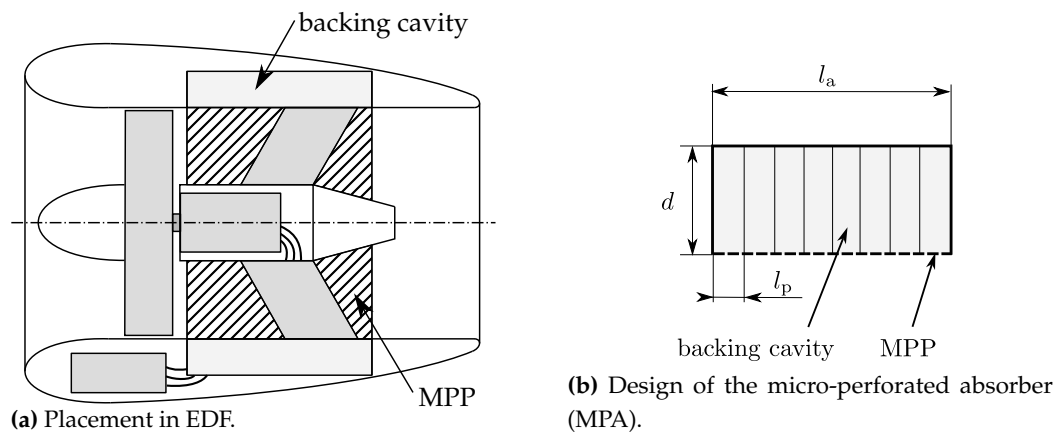


**Figure 4.** Design and placement of absorber linings.

The micro-perforated face sheet of the liner has a perforation rate  $\epsilon = 0.152$  and thickness  $t = 0.7$  mm. The perforations are slit-shaped. The absorber liner uses a backing cavity depth of  $d = 40$  mm, which already pushed the geometric limits of the fan unit's aerodynamic shell. The extent is also limited towards the inlet lip due to the avoidance of absorbers in the rotor plane, which would reduce the fan's aerodynamic efficiency [41]. The computed absorption maximum [42] in the lower frequency range at 1800 Hz is close to the fan unit's BPF at OP4 (see Table 3), which represents the maximum tonal SPL for the examined operating range. The highest broadband SPL will also be partially absorbed by the absorber designed, as the second maximum of the absorption coefficient occurs at 5500 Hz. As shown in Figure 4, the backing cavity of the absorber linings designed is partitioned to increase the absorption of random incident sound pressure waves. A partitioning resulted in the rectangular segment cross-sections, which were dimensioned according to former research insights [43]. The absorber linings were placed in the stators guide vane section duct to not disturb the aerodynamics at the rotor tip section. This placement resulted in a relative absorption area of 16.6% of the total inner duct area.

### 3. Measurement campaign for early prototyping

One of the most important acoustic indicators to determine a machine's acoustic emissions is the acoustic power level, which can be quantified by the enveloping surface method (ESM) to determine the sound power level of an acoustic source using an anechoic measuring room. The international standard *DIN EN ISO 3745* contains all the necessary information and procedures to conduct the

measurements needed for accuracy class 1. As the claims to the anechoic room have to be proven according to *ISO 26101* and are very restrictive, measurements for accuracy class 1 cannot be taken without unreasonable effort and are contradictory to the motivation of the study in providing an affordable experimental setup. However, a measuring method with the lower accuracy class 2 is described in the international standard *DIN EN ISO 3744* and can be conducted with fewer resources. The criteria of 15dB difference between external noise and the measured sound is met at all narrowband measurements [5].

3.1. Operation condition

The EDF units’ acoustic emissions are studied at four operating points, defined in [Table 3](#).

**Table 3.** The studied operating points of the EDF unit.

operating point	$f_{rot}$	$M_{tip}$	$f_{BPF}$	$f_{LF}$
OP 1	$6000\text{min}^{-1}$	0.18	700 Hz	1400 Hz
OP 2	$8000\text{min}^{-1}$	0.24	933 Hz	1866 Hz
OP 3	$10\,000\text{min}^{-1}$	0.30	1167 Hz	2343 Hz
OP 4	$12\,000\text{min}^{-1}$	0.36	1400 Hz	2800 Hz

The subsonic behavior of the observed EDF unit is evident when looking at the rotor blades’ tip Mach number  $M_{tip}$ . The temperature was about 26°C, the relative humidity 30%, and the atmospheric pressure was 98 kPa during the calibration and measurement. The microphones were calibrated according to the procedure described in [44]. The EDF is mounted at a fixed location inside a measurement room.

3.2. Measurement facility

Sound power measurements based on *DIN EN ISO 3744:2011-02* were carried out in a fully equipped low-reflection room with a reflecting floor [45].

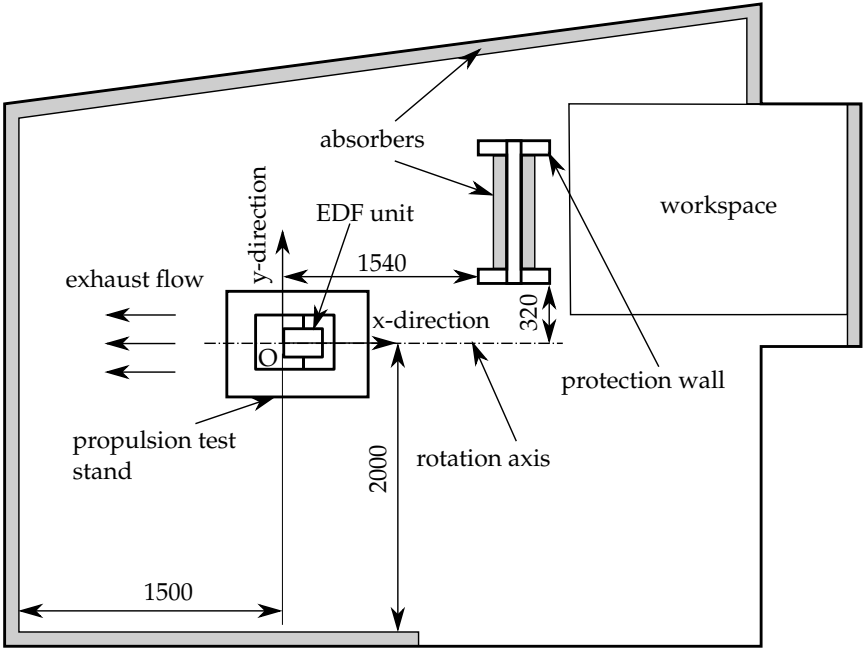


**Figure 5.** Setup and spatial dimensions of the experimental facility and positioning of the EDF unit on a propulsion test bench inside the measuring room. Adapted from [5].



A porous absorber (Baso Plan 100) is attached to approximately 50% of the room's walls and ceiling to produce relatively cheap, easy-to-install, and effective absorption characteristics. Mobile protection walls were needed to be put up to ensure safety for the people present in the measuring room during the EDF unit's operation. The acoustic properties of the facility limit the reliable experiments to frequencies above 300 Hz [45]. The room was characterized by reverberation time measurements in [5,44].

Ten microphones envelop the EDF unit by spanning a half-sphere surface around it [45] (see Figure 6).

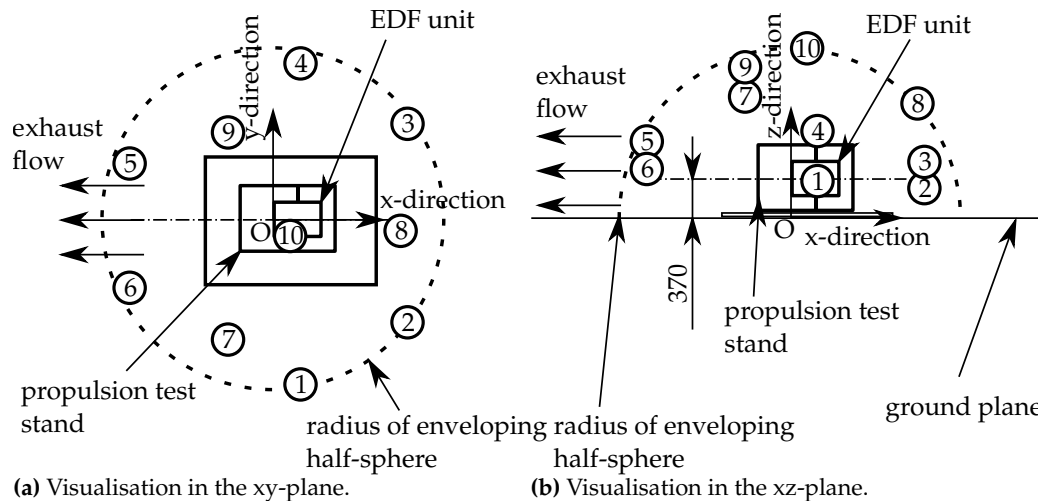


**Figure 6.** Visualisation of the microphone positions for the measurements relative to the propulsion test stand.

The EDF unit was mounted on a thrust measurement test rig. Figure 5 shows the EDF unit positioned inside the middle of the room to minimize the effects of flow interaction with the surrounding walls. In the current setup, no free flow conditions could be realized. The exhaust flow hits the rear wall, covered by acoustic absorber material, at a distance of 1.5 m. No avoiding measures to reduce the impinging jet on the room walls were used during the experiments. The measurement campaign produced reliable results since the goal was to understand the noise mechanisms and a possible mitigation strategy by comparing two manufactured variants.

The measurement concept followed the data processing presented in [44]. Pre-polarised back-electret condenser microphones (Sennheiser KE 4-211-2) with windscreens recorded the acoustic signal. According to the manufacturer, the capsule has high long-term stability and a constant sensitivity in the frequency range from 20 to 20000 Hz (within a deviation 3 dB). The signals emitted by the microphone capsules pass through the microphone-integrated preamplifier to the main amplifier (in-house developed amplifier, so-called FlexAmplifier), in which the signals can be amplified by a factor of 55 to 430, depending on the setting. The signals are amplified to achieve the recommended output level of the A/D converter (RM M32 AD). The digitized data is transferred to the MADiface (MADiface XT) via a fiber optic cable (LWL), where the signal is converted into the MADI format. The MADiface is connected to the computer via USB. Finally, the data is read and processed in MATLAB using the ASIO driver.

The measurements were sampled at a frequency of  $f_s = 48$  kHz. Each operating point was measured for 20 s. The data is further processed by the Matlab-based AcouCam-Software [44]. The measurement results were corrected with the measuring room's reverberation characteristics and the individual microphones' frequency-dependent sensitivities based on the data generated in [44]. Finally, the A-weighted sound power level spatially averaged across all microphone positions  $\overline{L_{W,A}}$  is computed.

### 3.3. Limitations and improvements

As already discussed above, this section additionally highlights possible limitations of the study in order to generate awareness and that the purpose of this study was not to tailor the measurements towards the highest accuracy but to stay within a minimal budget and to compare different configurations of the same EDF unit with an identical setup. The reproducibility was therefore tested during the experimental investigations and found to be the case within 1 dB(A) range.

A major improvement to the current study would be to perform countermeasures to the impinging jet on the room's walls and avoid large recirculations. Mitigating this was not possible in the available measurement facilities. The microphone positions were selected such that the influence of the airflow was kept to a minimum. Moreover, recirculations can affect the acoustic measurement and should be avoided using a relatively large room [15].

The authors are aware of the influence of ingested external disturbances, as they could strongly affect acoustic behavior. The problems first arose when comparing the acoustic data of jet engines gathered through ground tests and in-flight measurements with different inflow conditions. When ground vortices, atmospheric turbulences, or other flow disturbances are ingested, they are experienced by the rotor for several revolutions due to the elongation of the flow medium in a streamlined direction. In conclusion, broadband noise and tonal noise components result from ingested external disturbances interacting with the rotor [46,47]. In the ground testing stage of the study, mitigating this effect is subject to more advanced testing.

Furthermore, the directivity of the EDF unit's acoustic emissions was considered unidirectional. Several publications mentioned that the radiation is not unidirectional and varies with frequency (e.g., see in [15,25]). Since the setup's directivity was not clear upfront in this very early prototyping study, the benefit of knowing the directivity of a possible setup not being put into further production may be too early in the design process. We recommend studying the directivity and adapting the measurement positions for a second follow-up study of an EDF unit passing this presented preliminary study.

Finally, the measurement facility has no option to emulate a dismounted fan configuration's load onto the electric motor during measurements without a fan. Emulating the reactions from the fan would be necessary for a very reliable experimental study of the electric motor and the electronics. Again, within this limited budget and the facilities available, this was not possible in the scope of the work, and it was decided to drive the electric motor without fan loading to gain at least some information about the electric drive system. For following up on this topic, it is recommended to emulate the fan loading by a second electric motor connected to the propeller shaft.

## 4. Sound Power Measurements Results

Regarding being executed in early prototyping, the results are presented in the historical order of the data acquisition to highlight the knowledge generation process and reasoning accordingly. Firstly, the initial EDF unit results are presented and followed by an intermediate conclusion to point out the direction of follow-up investigations. After that, the noise emitted by the electric motor and controller is investigated without the fan being mounted. Finally, an acoustic treatment based on micro-perforated liners is presented to absorb the sound emissions partly.

### 4.1. Initial campaign

The measurements of the EDF were performed at four operating points and evaluated as narrowband-signals  $\overline{L_{W,A}}$  in Figure 7. The highest tonal sound power levels (SWL) are at the BPF and its harmonics at all operating points. The primary acoustic source mechanism at the BPF is an aerodynamic effect. In contrast, the higher harmonic frequencies (e.g., first, third, fifth) of the BPF could result from the electric powertrain since the number of pole pairs coincides with the number of blades. At OP1, the highest tonal SWL is at the third harmonic frequency of the BPF at 2.1 kHz. This strong SWL at the third harmonic frequency could result from the matching excitation and the aerodynamic

and electrodynamics forcing of the rotor structure. Literature suggests that this unusual amplification of the acoustic is possibly by a duct mode resonance [12,15]. The duct mode was confirmed by a 2D eigenmode simulation [48] using openCFS [49] and the influence of the flow was corrected according to [50]. Also noteworthy is that at OP1, a hump between the BPF and the first harmonic occurs.

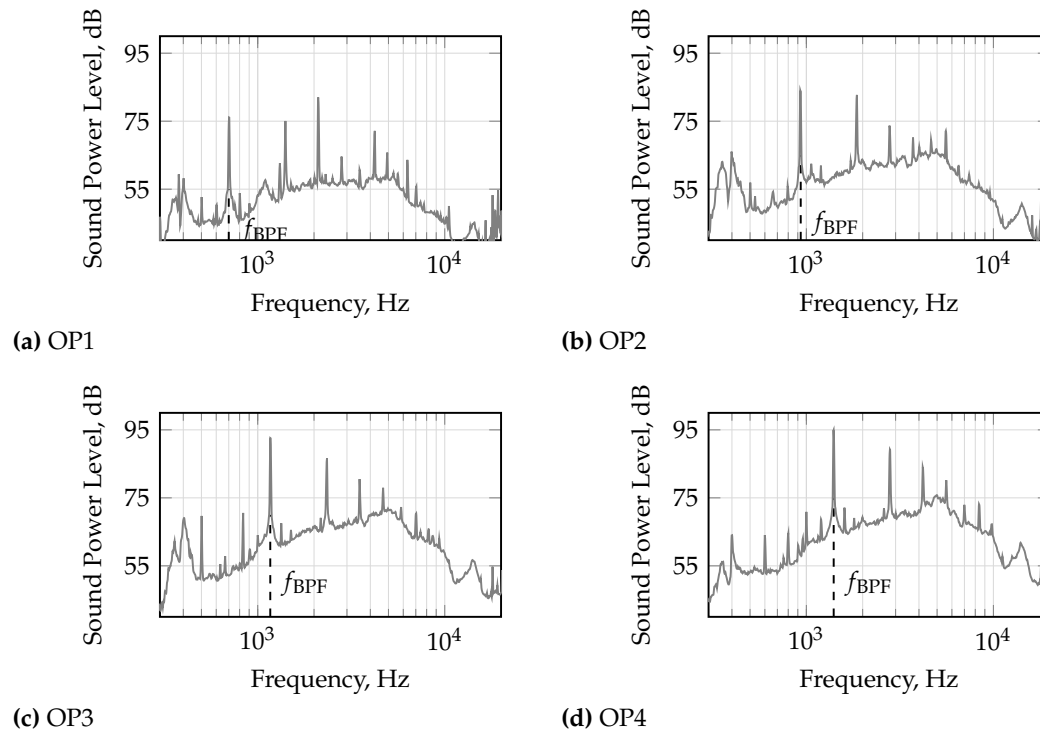


**Figure 7.** Narrowband  $\overline{L_{W,A}}$  at different operating points relative to the highest narrowband sound power level in the observed operating range.

High broadband components of the SWLs occur between 4 kHz to 6 kHz and grow in magnitude with increasing rotational speed. In [29], it is shown that both tip noise and boundary layer noise contribute to the broadband noise emissions of axial fans.

High narrowband components of the frequency spectrum are at 350 Hz to 450 Hz. They do not change in their frequency with increasing rotational speed. One hypothesis for the noise mechanism of those low-frequent narrowband components can be acoustic resonances of the electric motor cavity because those narrowband components have also been detected in subsequent measurements of the EDF's electric powertrain. Additionally, acoustic resonances of this kind have already been detected in [34]. An accompanying acoustic simulation confirmed that this hump is a duct mode.

Frequency components at 15 kHz do not depend on the rotational speed and are most likely caused by transistor operations of the electronic motor controller to achieve the electric phase commutation [27,28]. This base frequency of the switching noise is a typical acoustic signature of an electric powertrain.

Additional experiments of the EDF unit's SWL were performed as transient run-ups with a constant speed increase. Measurements between the neighboring operating points took 40 s using the setup as presented for the four stationary operation point experiments. Figure 8 shows the BPF and its harmonics as linearly increasing high SWL lines. This confirms the presence of aerodynamic sources at the BPF and its harmonics in the form of a rotor and a rotor-stator interaction.

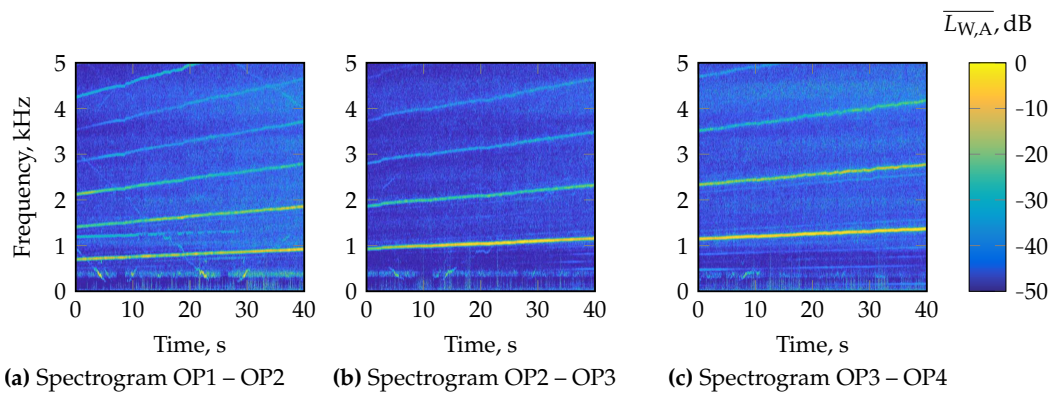


**Figure 8.**  $\overline{L_{p,A}}$  of the EDF unit, run between neighboring operating points. The scale is selected relative to the highest sound power level in the respective measurement range.

As already recognized in Figure 7 and confirmed by the results depicted in Figure 8, the narrowband SWL hump between 350 Hz and 450 Hz is independent of the operating condition. Between OP1 and OP3, repeating artifacts are visible that depend on the rotational speed piecewise linearly [27,28]. Those artifacts are most visible in Figure 8a and Figure 8b at about 400 Hz as linearly decreasing with the rotational speed, vanishing, and as the rotational speed increases further linearly increasing again. Four of those characteristics are identified between OP1 and OP3. The first occurs in Figure 8a disappearing from 5 s to 10 s, the second one in Figure 8a between 23 s and 30 s, the third one in Figure 8b between 6 s and 13 s and the fourth one in Figure 8c between 1 s and 8 s. A review of the literature [27,28] attributes this to the switching of the ECM.

At 1200 Hz a speed-independent single tonal component (see Figure 8a). Its amplitude decays with increasing fan speed and completely disappears after 30 s. An aerodynamic resonance of the EDF unit can describe this behavior.

Finally, the reproducibility of the measurement was investigated by comparing the post-processed results of the two measurements in Figure 9. The difference between both measurement series was less than 1 dB over the whole operating range. Interestingly, specific humps occur around 6300 and 9000 revolutions per minute in this data.

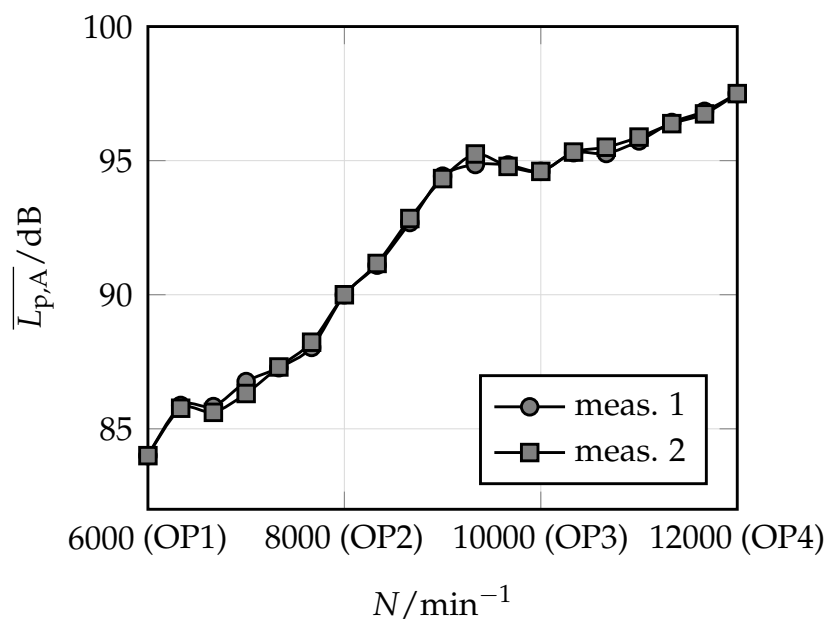


**Figure 9.** A-weighted OSPL of unmodified EDF unit over operating range.

The two bumps in Figure 9 can be explained by the unusual amplification by an acoustic resonance, coinciding the third BPF at about 6300 revolutions. Since it also can explain the second hump occurring at about 9000 revolutions per minute, this is a further hint towards an acoustic resonance of the duct at about 2.1 kHz. As intended by the perforated liner design presented in the previous section, frequencies around 2.1 kHz are absorbed and are an effective countermeasure to reduce this resonant effect occurring at 2.1 kHz.

#### 4.2. Intermediate conclusion

Based on these initial results, some odd dependencies of frequencies on the revolutions of the fan are questionable and may be further investigated. Firstly, a more in-depth investigation targets the switching noise of the electric motor and the EMC. Therefore, the electric powertrain is investigated transiently with a dismounted aerodynamic rotor. The same operating range was considered for this study.

Secondly, the explanation for the humps in Figure 9 and how they can be mitigated is of interest. The motor has 14 Poles, which can interact with the seven blades rotor structure and overlap the second BPF with some electrodynamics excitation of the rotor structure. This coincidence has to be evaluated and might be a reason for the amplification of the third harmonics of the BPF, but it cannot explain the amplification of the second hump at 9000 revolutions in Figure 9 and therefore, we are confident that this is connected to an acoustic mode based on the preliminary data. Another possibility can be a structural mode of the duct. Any absorber placement inside the duct modulates the acoustic emissions by absorption and changes structural modes of the duct by the updated geometry. Therefore, we will see an impact on these humps by the absorber placement.

#### 4.3. Effects of the electric drive

Regarding the intermediate conclusion on the ECM noise, the fan was removed to detect the odd behavior of some noise emissions. Additionally, we investigate the proportion of the noise that comes from the EDF electric powertrain without the fan's influence. By dismounting the fan, the noise emissions of the electric powertrain can be studied, but no direct comparison with the previously presented setup is possible. In the case without load, the ECM's internal currents and electromagnetic forces are significantly lowered than in the loaded case. Therefore, we expect lower absolute SPL amplitudes for the components under load, which makes a direct comparison impossible. Nevertheless, a first insight can be gained into the relevant frequency content of the acoustic spectrum. Additionally, noise compensation based on physical considerations regarding the electric current would be possible by advanced countermeasures [27,28].

Figure 10 shows the SWL results of the measurement campaign at the considered operating points. The powertrain's highest tonal noise emissions quantified at OP1 without load occur at 2.1 kHz. This coincides with the EDF unit's third harmonic of the BPF. The electric powertrain in clogging torque characteristics is responsible for this tonal noise component. As mentioned, the amplification can also result from a structural or acoustic duct mode. The result further emphasizes that some natural frequency is present there. The highest recognized tonal SWLs of the electric components happened at multiples of the rotational motor speed, which supports the hypothesis of electromagnetic forces being an important noise generator to be considered. Since the narrowband SWLs between 350 Hz and 450 Hz are also pronounced in this measurement study, an aerodynamic mechanism as origin can be excluded as a root of this noise. Most likely, the acoustic duct mode is responsible for the modulation. In [34], an acoustic resonance of the motor's internal airspace between its rotor and stator was causing these narrowband SWLs, independent of the rotational speed.

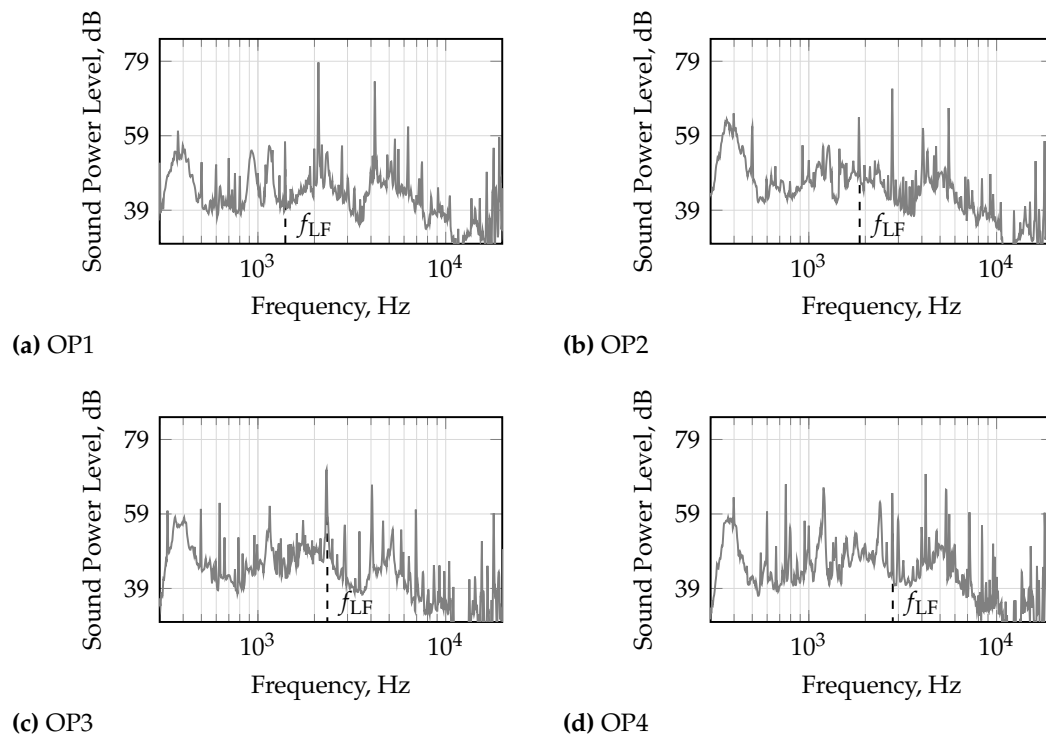


**Figure 10.** Narrowband  $\overline{L_{W,A}}$  of the electric powertrain with dismounted axial fan stage operated at four operating points.

In OP1 of Figure 7, the highest tonal SWL exists at the third BPF harmonic (and at the first harmonic of the pole forces), indicating an unusual amplification of the acoustic and structural components by a natural frequency. At this frequency, the SWLs are pronounced when considering only the acoustic results of the electric powertrain. In this OP1, the electric powertrain emissions are associated with the first harmonic of the electrodynamic pole forces and are modulated by coincidence with the duct mode at 2.1 kHz.

Run-up measurement studies for the operating range between OP1 and OP4 were carried out for the unloaded EDF unit. Figure 11 shows spectrograms to visualize the powertrain's noise dependence on the motor speed. We observe in Figure 11 that controlling difficulties of the unloaded EDF unit occurred. As a result, the rotational speed was only block-constant across the entire operating range. Tonal noise components at the primary electromagnetic frequency  $f_{LF}$  and their harmonics are notably visible by linearly increasing lines.

The previously discussed artifact is now more pronounced. Both increasing and decreasing frequency characteristics with increasing rotational speed are observable in the measurement results. According to the literature [27,28], the electric drives' commutation operating principle of the inverter is responsible for this noise characteristic. However, a closer examination of the electronic components, cooling fin vibrations and the electric motor supply current needs to be conducted to prove this hypothesis [28].



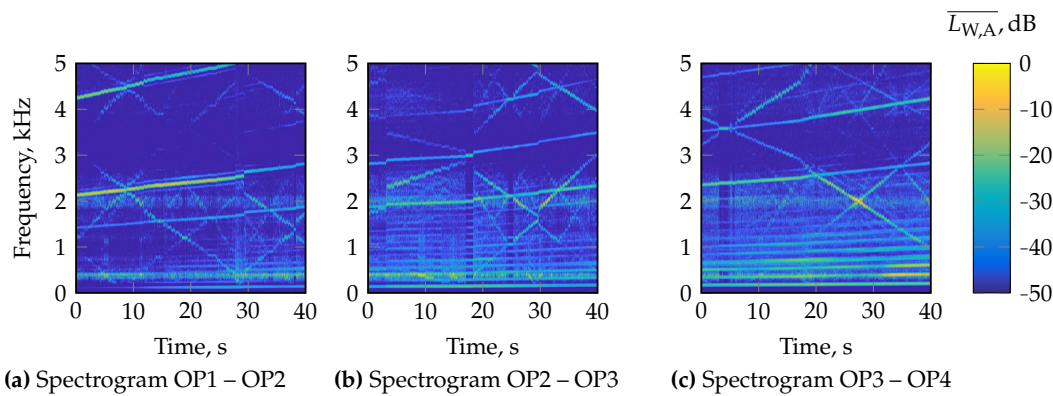


**Figure 11.**  $\overline{L_{p,A}}$  of the electric powertrain between neighboring operating points relative to the highest sound power level in the respective measurement range.

Another interesting aspect, revealed by the data presented in Figure 11, is that a revolution-independent signature occurs at 2.1 kHz. As indicated previously for OP1, this overlaps with the electrodynamics forcing of the motor (as visible in Figure 11a). Furthermore, the 2.1 kHz modulation also amplifies the x-shaped characteristics of the electronics switching the motor currents at around 30 s between OP3 and OP4 in Figure 11c.

#### 4.4. Effects of the Perforated Liner

Regarding the previous measurement campaigns and according to the description, the EDF unit design was modified by placing acoustic liners inside the duct. These micro-perforated liners were used to reduce the operating range's emitted sound power overall, especially around 2.0 kHz. Based on the two design variants (unmodified and modified duct), the A-weighted overall sound power level (OSPL) was measured, computed, and compared (see Figure 12). The design of the micro-perforated liners was performed based on experience and without optimizing the position and the design concerning noise mitigation, the placement of the acoustic liners decreased the emitted noise over a broad operating range. The design was constructed in order to absorb the acoustic energy around 2.0 kHz and 5.5 kHz best. The influence on the discussed attenuation humps at 2.1 kHz in the OSPL was expected and is observable in Figure 12. Exemplarily, for the narrowband SWL, the unmodified and the modified EDF unit are compared in Figure 12. A reduction of several dB is observable at the tonal components, with a more significant reduction at the second BPF, which is close to the first absorber design absorption maximum at 2.0 kHz. Accompanying spectrograms of modified EDF unit are given in Figure 13.

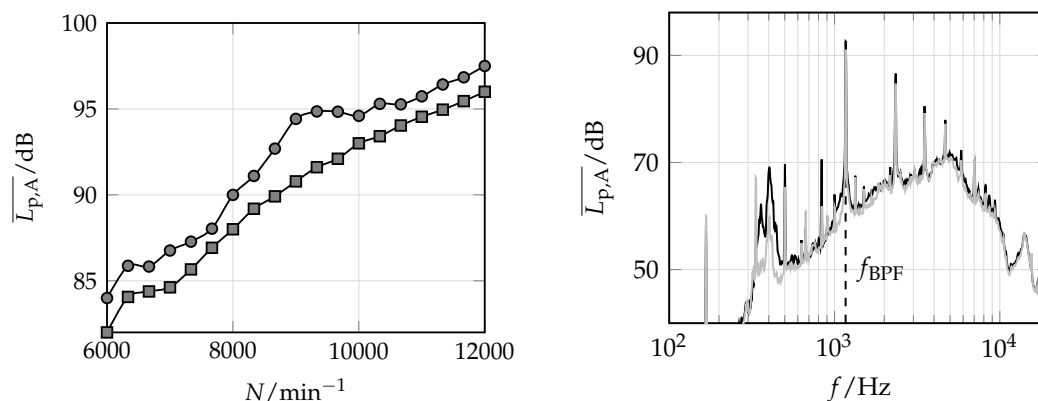


**Figure 12.** A-weighted OSPL over operating range of unmodified (●) and modified (■) and the narrowband  $\overline{L_{p,A}}$  of EDF unit at OP3 with black the unmodified and gray the modified configuration.

As already explained, the small hump at 6300 revolutions in the A-weighted OSPL (see Figure 12) is an interrelation between the 3rd harmonic of the BPF and the base frequency. A reduction of the hump is within the range of the overall reduction of the OSPL. Noteworthy is that the small maximum disappeared, which is attributed to the modulation of the resonance occurring at 2.1 kHz. At the second, more pronounced hump located at 9000 revolutions per minute, the A-weighted OSPL was reduced significantly by 4 dB(A). As indicated, this hump resulted from a resonance occurring at 2.1 kHz, effectively modulated by the designed micro-perforated liner. Instead of the unmodified EDF unit, the modified EDF unit now has an expected behavior that the OSPL is increasing monotonously and linearly in the dB scale with increasing revolutions. Overall, the A-weighted OSPL was reduced by 2-4 dB across the total operating range of the EDF unit, whereas specific narrowband tonal frequencies were decreased stronger.

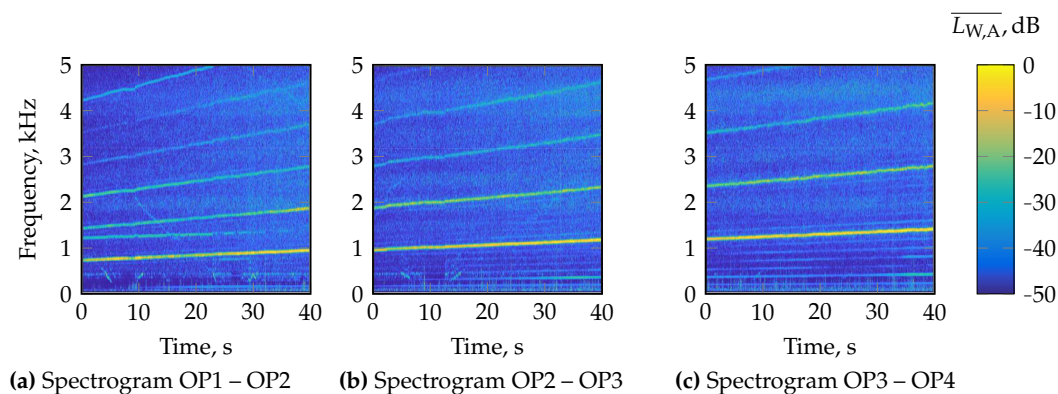


**Figure 13.** Spectrograms in the operating range of the modified EDF unit.

Finally, the reported subharmonic hump reported for OP1 vanished with the absorber treatment [5].

## 5. Conclusion and Suggestions

In this acoustic measurement campaign for early prototyping, we showed how to achieve reliable results within a limited budget and timeframe. The study of the EDF unit's noise emissions in the investigated operating range has shown expected tonal components at the BPF and its harmonics. Aerodynamic reasons caused the highest measured sound power levels. An unexpected excitation and duct mode frequency match caused specific humps on the overall sound power level measurements.

In contrast, minor sound power level characteristics in the spectrogram could be attributed to the electric powertrain and its components. The fundamental frequency of the ECM's electromagnetic forces caused tonal noise emissions of the electric powertrain with a dismounted axial fan. X-shaped dependence on the rotational speed of tonal noise emissions in spectrograms was found for transient measurements of the electric powertrain. The behavior was assigned to the switching currents of the electric powertrain. Regarding the measurement results of the electric powertrain in contrast to the entire EDF unit, a study using an artificial loading to account for the original fan load would be interesting to make the results comparable. Furthermore, the next measurement campaign is motivated to adjust the test rig to analyze the electric powertrain's effects. In the future, a detailed analysis of the electric powertrain would also involve measurement of the individual single motor phases and currents supplied to the motor. These correlations could be drawn to understand the powertrains' noise emissions better.

Given the EDF's acoustic characteristics findings, perforate absorber linings were laid out to effectively absorb the sound pressure waves with the highest amplitude, which the BPF represents. After designing and manufacturing the absorber linings, the modified EDF was measured again and a resulting reduction in the SPL was noticed. The A-weighted OSPL was reduced by 2-4 dB across the

EDF operating range, whereas the dominant BPF and the harmonics were attenuated by up to 10 dB. Although discussed limitations to the affordable measurement campaign apply, gaining first insight in early prototyping is valuable and can be combined with more detailed computational or experimental studies. The value of the method was proven by identifying the EDF's noise characteristics of an improved design version and lowering the overall noise signature by several dB across a wide operating range.

**Acknowledgments:** Supported by TU Graz Open Access Publishing Fund.

## References

1. ICAO. 2022 Environmental Report. <https://www.icao.int/environmental-protection/Pages/envrep2022.aspx>, 2022. [Online; accessed 12-Oct-2022].
2. Organization, W.H.; et al. *Environmental noise guidelines for the European region*; World Health Organization. Regional Office for Europe, 2018.
3. Pascioni, K.; Rizzi, S.A. Tonal noise prediction of a distributed propulsion unmanned aerial vehicle. In Proceedings of the 2018 AIAA/CEAS Aeroacoustics Conference, 2018, p. 2951. <https://doi.org/10.2514/6.2018-2951>.
4. Kim, H.D.; Perry, A.T.; Ansell, P.J. A review of distributed electric propulsion concepts for air vehicle technology. In Proceedings of the 2018 AIAA/IEEE Electric Aircraft Technologies Symposium (EATS). IEEE, 2018, pp. 1–21.
5. Schmidt, J. Acoustic optimisation of an electric ducted fan unit through absorber design and placement, 2020. <https://doi.org/10.34726/hss.2020.75042>.
6. Pereira, J.L. *Hover and wind-tunnel testing of shrouded rotors for improved micro air vehicle design*; University of Maryland, College Park, 2008.
7. Raeisi, B. AERODYNAMIC STUDY OF TILTING ASYMMETRICAL DUCTED FANS MOUNTED AT THE WING TIPS OF A VTOL UAV. PhD thesis, Ryerson University, 2016.
8. Abrego, A.I.; Bulaga, R.W.; Rutkowski, M. Performance study of a ducted fan system. In Proceedings of the American Helicopter Society Aerodynamics, Acoustics and Test and Evaluation Technical Specialists Meeting, 2002.
9. Rhee, W.; Myers, L.; McLaughlin, D. Aeroacoustics of vertical lift ducted rotors. In Proceedings of the 15th AIAA/CEAS Aeroacoustics Conference (30th AIAA Aeroacoustics Conference), 2009, p. 3333.
10. Yilmaz, S.; Erdem, D.; Kavsaoglu, M.S. Performance of a ducted propeller designed for UAV applications at zero angle of attack flight: An experimental study. *Aerospace Science and Technology* **2015**, *45*, 376–386.
11. Zhang, T.; Barakos, G.N. Review on ducted fans for compound rotorcraft. *The Aeronautical Journal* **2020**, *124*, 941–974. <https://doi.org/10.1017/aer.2019.164>.
12. Malgoezar, A.M.; Vieira, A.; Snellen, M.; Simons, D.G.; Veldhuis, L.L. Experimental characterization of noise radiation from a ducted propeller of an unmanned aerial vehicle. *International Journal of Aeroacoustics* **2019**, *18*, 372–391.
13. Hall, C.A.; Crichton, D.; et al. Engine and installation configurations for a silent aircraft. *ISABE* **2005**, *1164*, 2005.
14. Hileman, J.; Spakovszky, Z.; Drela, M.; Sargeant, M. Airframe design for "silent aircraft". In Proceedings of the 45th AIAA Aerospace Sciences Meeting and Exhibit, 2007, p. 453.
15. Weintraub, D.; Koppelberg, J.; Köhler, J.; Jeschke, P. Ducted fans for hybrid electric propulsion of small aircraft. *CEAS Aeronautical Journal* **2022**, *13*, 471–485.
16. Ko, A.; Ohanian, O.; Gelhausen, P. Ducted fan UAV modeling and simulation in preliminary design. In Proceedings of the AIAA modeling and simulation technologies conference and exhibit, 2007, p. 6375.
17. Moore, M.D. Misconceptions of electric aircraft and their emerging aviation markets. In Proceedings of the 52nd Aerospace Sciences Meeting, 2014, p. 0535.
18. Casagrande Hirono, F.; Torija Martinez, A.; Elliott, A.; Taylor, J.; Grimshaw, S.; Lefas, D. Aeroacoustic design and optimisation of an all-electric ducted fan propulsion module for low-noise impact. In Proceedings of the 28th AIAA/CEAS Aeroacoustics 2022 Conference, 2022, p. 3034.

19. Rizzi, S.A.; Huff, D.L.; Boyd, D.D.; Bent, P.; Henderson, B.S.; Pascioni, K.A.; Sargent, D.C.; Josephson, D.L.; Marsan, M.; He, H.B.; et al. Urban air mobility noise: Current practice, gaps, and recommendations. Technical report, 2020.
20. Schoder, S.; Schmidt, J.; Furlinger, A.; Kaltenbacher, M. Quantification of the Acoustic Emissions of an Electric Ducted Fan Unit. In Proceedings of the 2022 Delft International Conference on Urban Air-Mobility: DICUAM 2022, 2022.
21. Darrah, D.; Eppler, J.; Liu, W.; Anemaat, W.A. Electric Ducted Fan Design and Testing for High Performance UAV Integration. In Proceedings of the AIAA Scitech 2020 Forum, 2020, p. 0017.
22. Schmidt, J.; Kaltenbacher, M.; Furlinger, A.; Schoder, S. Experimental Characterization of an Electric Ducted Fan Unit's Acoustic Emissions. In Proceedings of the AIAA AVIATION 2021 FORUM, 2021, p. 2174.
23. Smith, M.J.T. *Aircraft Noise*; Cambridge Aerospace Series, Cambridge University Press, 1989. <https://doi.org/10.1017/CBO9780511584527>.
24. Moreau, S. A review of turbomachinery noise: from analytical models to high-fidelity simulations. *Fundamentals of High Lift for Future Civil Aircraft* **2021**, pp. 579–595.
25. Schoder, S.; Junger, C.; Kaltenbacher, M. Computational aeroacoustics of the EAA benchmark case of an axial fan. *Acta Acustica* **2020**, *4*, 22. <https://doi.org/10.1051/aacus/2020021>.
26. Vijayraghavan, P.; Krishnan, R. Noise in electric machines: A review. *IEEE Transactions on Industry Applications* **1999**, *35*, 1007–1013.
27. Sarrazin, M.; Anthonis, J.; Van der Auweraer, H.; Martis, C.; Gyselinck, J. Signature analysis of switched reluctance and permanent magnet electric vehicle drives. In Proceedings of the 2014 International Conference on Electrical Machines (ICEM). IEEE, 2014, pp. 1831–1837.
28. Fang, Y.; Zhang, T. Sound quality investigation and improvement of an electric powertrain for electric vehicles. *IEEE Transactions on Industrial Electronics* **2017**, *65*, 1149–1157.
29. Krömer, F.J. *Sound emission of low-pressure axial fans under distorted inflow conditions*; FAU University Press, 2018. <https://doi.org/10.25593/978-3-96147-089-1>.
30. Tyler, J.M.; Sofrin, T.G. Axial flow compressor noise studies. Technical report, SAE Technical Paper, 1962. <https://doi.org/10.4271/620532>.
31. Griffiths, J. The spectrum of compressor noise of a jet engine. *Journal of Sound and Vibration* **1964**, *1*, 127–140. [https://doi.org/10.1016/0022-460X\(64\)90074-4](https://doi.org/10.1016/0022-460X(64)90074-4).
32. Gieras, J.F.; Wang, C.; Lai, J.C. *Noise of polyphase electric motors*; CRC press, 2018. <https://doi.org/10.1201/9781420027730>.
33. Ko, H.S.; Kim, K.J. Characterization of noise and vibration sources in interior permanent-magnet brushless DC motors. *IEEE Transactions on Magnetics* **2004**, *40*, 3482–3489. <https://doi.org/10.1109/TMAG.2004.832991>.
34. Lee, H.J.; Chung, S.U.; Hwang, S.M. Noise source identification of a BLDC motor. *Journal of mechanical science and technology* **2008**, *22*, 708–713. <https://doi.org/10.1155/2015/879581>.
35. Pindoriya, R.; Mishra, A.; Rajpurohit, B.; Kumar, R. An analysis of vibration and acoustic noise of BLDC motor drive. In Proceedings of the 2018 IEEE Power & Energy Society General Meeting (PESGM). IEEE, 2018, pp. 1–5. <https://doi.org/10.1109/PESGM.2018.8585750>.
36. Neise, W.; Michel, U. Aerodynamic noise of turbomachines. *Deutsche Forschungsanstalt für Luft-und Raumfahrt, eV, DLR, Institut für Strömungsmechanik, Abt. Turbulenzforschung, Berlin* **1994**, *5*.
37. Hubbard, H.; Lansing, D.; Runyan, H. A review of rotating blade noise technology. *Journal of Sound and Vibration* **1971**, *19*, 227–249.
38. Copeland, W.; Crigler, J. Experimental noise studies of inlet-guide-vane-rotor-stator interactions for a single-stage axial-flow compressor. Technical report, 1965.
39. Krömer, F.; Czwielong, F.; Becker, S. Experimental investigation of the sound emission of skewed axial fans with leading-edge serrations. *AIAA Journal* **2019**, *57*, 5182–5196.
40. Krömer, F.J.; Moreau, S.; Becker, S. Experimental investigation of the interplay between the sound field and the flow field in skewed low-pressure axial fans. *Journal of Sound and Vibration* **2019**, *442*, 220–236.
41. Floss, S. Minderung von Schallausbreitung durch Mikroperforierte Absorber in unterschiedlichen Schallfeldarten-Design und Evaluierung. PhD thesis, Wien, 2022. <https://doi.org/10.34726/hss.2022.57522>.
42. Jaouen, L.; Bécot, F.X. Acoustical characterization of perforated facings. *The Journal of the Acoustical Society of America* **2011**, *129*, 1400–1406.

43. Liu, J.; Herrin, D. Enhancing micro-perforated panel attenuation by partitioning the adjoining cavity. *Applied Acoustics* **2010**, *71*, 120–127.
44. Gombots, S. Acoustic source localization at low frequencies using microphone arrays. PhD thesis, Wien, 2020.
45. DIN EN ISO 3744: 2011-02: Akustik – Bestimmung der Schallleistungs- und Schallenergiepegel von Geräuschquellen aus Schalldruckmessungen – Hüllflächenverfahren der Genauigkeitsklasse 2 für ein im Wesentlichen freies Schallfeld über einer reflektierenden Ebene (ISO 3744: 2010). Standard, Beuth-Verlag, Berlin, DE, 2011.
46. FEILER, C.; GROENEWEG, J. Summary of forward velocity effects on fan noise. In Proceedings of the 4th Aeroacoustics Conference, 1977, p. 1319.
47. Groeneweg, J.; Rice, E. Aircraft turbofan noise **1987**.
48. Maurerlehner, P.; Schoder, S.; Tieber, J.; Freidhager, C.; Steiner, H.; Brenn, G.; Schäfer, K.H.; Ennemoser, A.; Kaltenbacher, M. Aeroacoustic formulations for confined flows based on incompressible flow data. *Acta Acustica* **2022**, *6*, 45.
49. Schoder, S.; Roppert, K. openCFS: Open Source Finite Element Software for Coupled Field Simulation–Part Acoustics. *arXiv preprint arXiv:2207.04443* **2022**.
50. Broatch, A.; García-Tíscar, J.; Roig, F.; Sharma, S. Dynamic mode decomposition of the acoustic field in radial compressors. *Aerospace Science and Technology* **2019**, *90*, 388–400.

**Disclaimer/Publisher’s Note:** The statements, opinions and data contained in all publications are solely those of the individual author(s) and contributor(s) and not of MDPI and/or the editor(s). MDPI and/or the editor(s) disclaim responsibility for any injury to people or property resulting from any ideas, methods, instructions or products referred to in the content.